BioChem Press

Inter*net* Electronic Journal of Molecular Design

October 2002, Volume 1, Number 10, Pages 503–526

Editor: Ovidiu Ivanciuc

Special issue dedicated to Professor Haruo Hosoya on the occasion of the 65th birthday
Part 2

Guest Editor: Jun–ichi Aihara

Microscopic Solvation and Spontaneous Ionization of Li in Small Polar Solvent Clusters: Theoretical Analysis of Photoelectron Spectra for $Li^-(NH_3)_n$ and $Li^-(H_2O)_n$ ($n = 1–4$)

Kenro Hashimoto, Kota Daigoku, Tetsuya Kamimoto, and Taku Shimosato

Computer Center and Department of Chemistry, Tokyo Metropolitan University, 1–1 Minami–Ohsawa, Hachioji–shi, Tokyo 192–0397 Japan

Citation of the article:
K. Hashimoto, K. Daigoku, T. Kamimoto, and T. Shimosato, Microscopic Solvation and Spontaneous Ionization of Li in Small Polar Solvent Clusters: Theoretical Analysis of Photoelectron Spectra for $Li^-(NH_3)_n$ and $Li^-(H_2O)_n$ ($n = 1–4$), *Internet Electron. J. Mol. Des.* **2002**, *1*, 503–526, http://www.biochempress.com.

Microscopic Solvation and Spontaneous Ionization of Li in Small Polar Solvent Clusters: Theoretical Analysis of Photoelectron Spectra for Li⁻(NH₃)ₙ and Li⁻(H₂O)ₙ (n = 1–4)[#]

Kenro Hashimoto,* Kota Daigoku, Tetsuya Kamimoto, and Taku Shimosato

Computer Center and Department of Chemistry, Tokyo Metropolitan University, 1–1 Minami–Ohsawa, Hachioji–shi, Tokyo 192–0397 Japan

Abstract

Motivation. The understanding of the electronic states of alkali atom embedded in small polar solvent clusters is indispensable to construct a microscopic model of solvation and dissolution of metals. In connection to the recent photoelectron spectroscopy of negatively charged $Li^-(NH_3)_n$ and $Li^- (H_2O)_n$, we have carried out *ab initio* study for n up to 4 to unveil the electronic change behind the n dependence of their spectra.

Method. The cluster geometries were investigated extensively by the second–order many–body perturbation method with the 6–311++G(d,p) basis sets. The vertical electron detachment energies for the transitions from the anionic ground state to the neutral ground and low–lying excited states were calculated by the multi reference single and double excitation configuration interaction method.

Results. The most stable structures of both $Li^-(NH_3)_n$ and $Li^-(H_2O)_n$ for each n tend to have as many Li–nonhydrogen bonds as possible. The size dependence of the vertical electron detachment energies for the 2^2S-, 2^2P- and 3^2S-type transitions at these geometries are in good agreement with the experiment. The valence electrons of Li are squeezed out of the solvation shell, giving rise to the spontaneous ionization of Li. The solvated Li^+ is surrounded by the diffused electrons in the $n \geq 3$ anions.

Conclusions. The spatial expansion of the unpaired electron distribution also occurs in the neutral states with increasing n. The growing one–center (Rydberg–like) ion–pair nature is responsible for the rapid decrease of the energy separations between the ground and the low–lying electronic levels of the neutrals, namely the red shifts of the higher photoelectron bands.

Keywords. Alkali metal; solvation; spontaneous ionization; photoelectron spectrum; Rydberg–like state.

Abbreviations and notations

CASSCF, Complete active space self consistent field	VDE, Vertical detachment energy
CPC, Counterpoise correction	PES, Photoelectron spectrum
EBE, Electron binding energy	ZPC, Zero point correction
MRSDCI, Multi reference single and double excitation configuration interaction	

---

1 INTRODUCTION

Solvation of metals is one of the fundamental research subjects in wide areas of physics, chemistry and biochemistry. The understanding of this phenomenon at the molecular level is important to construct a microscopic model for spontaneous electron transfer from metal to solvent and formation of solvated electron. Clusters containing a single alkali atom and polar solvents have thus been investigated intensively in recent years [1,2]. Spectroscopic studies give essential information about the size dependence of the electronic levels of the clusters, and the photoionization threshold measurement of $M(H_2O)_n$ and $M(NH_3)_n$ (M=Na[3], Cs[4] and Li[5,6]) motivated many theoretical works [7–16].

Another approach to probe the electronic ground and low–lying excited states of the clusters is the photoelectron spectroscopy of negatively charged species. Takasu *et al*. recorded the photoelectron spectra (PESs) of $Na^-(NH_3)_n$ ($n \leq 12$) and $Na^-(H_2O)_n$ ($n \leq 7$) [6,17]. In the PESs of $Na^-(NH_3)_n$, the position of the first band derived from 3^2S (Na) $\leftarrow$ 3^1S (Na$^-$) transition is red–shifted from 0.55 eV to ca. 0.4 eV for $n = 1 \leftarrow 0$, and becomes almost constant for larger n. The second band for the transition to the 3^2P (Na)–like state is shifted rapidly to the lower electron binding energy (EBE) from 2.65 eV ($n = 0$) to 1.26 eV ($n = 4$) and further with much slower rate with increasing n. In contrast, both first and second photoelectron bands for $Na^-(H_2O)_n$ are blue–shifted by keeping their separation almost unchanged as n grows. The amount of the shifts becomes as large as 1.0 eV at $n = 7$.

They have also found that the interesting similarity and dissimilarity of the PESs are observed when Na^- is replaced by Li^- [5,6,18]. The first PES band of $Li^-(NH_3)_n$ is red–shifted only gradually from the atomic $2^2S(Li)$ $\leftarrow$ $2^1S(Li^-)$ transition (0.62 eV) to ~0.45 eV for $1 \leq n \leq 4$. It stays nearly constant for $n \leq 11$ but is shifted back gradually to higher EBE for $11 \leq n \leq 16$. The second band is down–shifted drastically from 2.47 eV ($n = 0$) to 1.22 eV ($n = 4$) and further for larger n. It almost superimposed on the 2^2S–type transition for $n \geq 10$. In addition, the weak third band whose size dependence is similar to that of the second band was observed. This behavior of the PESs is essentially similar to that of $Na^-(NH_3)_n$ at least for $n \leq 4$. On the other hand, the EBEs of the first and second PES bands for $Li^-(D_2O)_n$ decrease by 0.09 eV and by 1.03 eV, respectively, from $n = 0$ to $n = 4$, but increase monotonically for $4 \leq n \leq 10$. The blue shifts at $n = 10$ from $n = 4$ are 0.19 eV and ~0.5 eV for the first and second bands, respectively. The size dependence of PESs for $Li^-(D_2O)_n$ is in sharp contrast to that of $Na^-(H_2O)_n$ but resembles those of $Na^-(NH_3)_n$ and $Li^-(NH_3)_n$, especially when n is smaller than 4.

In the previous works [19–21], we have investigated $Na^-(NH_3)_n$ and $Na^-(H_2O)_n$ ($n \leq 4$) by *ab initio* MO method. The most stable structures of $Na^-(NH_3)_n$ ($n \leq 4$) are similar to those of the neutrals with the same n. Na tends to have as many Na–N bonds as possible in both anionic and neutral states. The observed decrease of the PES band separation has been ascribed to the growing

one–center (Rydberg–like) ion–pair nature in the clusters. In $Na^-(H_2O)_n$, hydrogen–bonded water clusters are bound to Na^- from H sides. At these geometries, the difference of the hydration energy between anionic and neutral states increases with n, and the electronic nature of the Na atom is only perturbed by waters in the neutrals, which results in the near parallel blue shifts of the PES bands.

We have also reported preliminary results on $Li^-(NH_3)_n$ and $Li^-(H_2O)_n$ ($n \leq 3$), and shown the near constancy of vertical electron detachment energies (VDEs) for the first band in the structure with maximum numbers of Li–N or Li–O bonds by the coupled cluster method [19]. In this work, we extend our research on these solvation clusters of Li^- with n up to 4 by examining the low–energy isomers extensively. The questions that we intend to answer are as follows: (1) Are the most stable isomers for each n also responsible for the higher PES bands? (2) Why the higher bands are shifted dramatically in both $Li^-(NH_3)_n$ and $Li^-(H_2O)_n$? (3) What electronic change does occur in $Li(NH_3)_n$ and $Li(H_2O)_n$ behind the PESs of their negatively charged species?

We will show that the higher PES bands observed for $Li^-(NH_3)_n$ and $Li^-(H_2O)_n$ are assignable to 2^2P- and 3^2S-type transitions in the structures where Li^- is surrounded by the solvents from nonhydrogen sides for all $n \leq 4$. The valence electrons of Li are squeezed out of the solvation shell, and the solvated Li^+ is surrounded by the diffused electrons in the $n \geq 3$ anions. The down shifts of the higher PES bands in both kinds of clusters are due to one–center (Rydberg–like) ion–pair nature grown by the stepwise solvation as in the case of $Na^-(NH_3)_n$. The structure dependence of the VDEs for $Li^-(NH_3)_n$ and $Li^-(H_2O)_n$ resembles that for $Na^-(NH_3)_n$ and $Na^-(H_2O)_n$. The similarity and dissimilarity of the PESs among the four kinds of clusters reflect the difference of their most stable anionic structures, namely, the electronic changes occurring in the clusters with increasing n.

2 METHOD

Molecular structures of $Li^-(NH_3)_n$ and $Li^-(H_2O)_n$ (n = 1–4) were optimized and harmonic vibrational analyses were carried out at the MP2/6–311++G(d,p) level with usual frozen core approximation[22] using Gaussian–98 program[23]. If an optimized structure, usually with some symmetry constraint, has one or more imaginary frequencies, we further optimized the structure following the imaginary normal modes until we reached the true local minimum.

Total binding energies, $\Delta E(n)$, were evaluated by the following formula:

$$-\Delta E(n) = E[[Li^-(Solv.)_n] - E[Li^-] - nE[Solv.] \qquad (Solv. = NH_3 \text{ or } H_2O). \qquad (1)$$

The zero point corrections (ZPC) were included in the $\Delta E(n)$ by using the scaled harmonic frequencies. The scale factors, 0.943(NH_3) and 0.953(H_2O), were obtained from the average ratios of the fundamental [24] and the calculated harmonic frequencies of a free solvent molecule. We assessed the basis set superposition errors for the $\Delta E(n)$ by the counterpoise correction (CPC).

The VDEs from the anionic ground state to the ground and low–lying excited states of neutrals

were calculated with MOLPRO–2000 program package [25]. We employed the multi reference single and double excitation configuration interaction (MRSDCI) method preceded by the complete active space self consistent field (CASSCF) calculations [26–29]. The active space for the CASSCF consists of five MOs corresponding to the $2s$, $2p$ and $3s$ orbitals of Li. In the CASSCF computations, the wavefunctions for the anions were optimized for the ground state, while the ground and four low–lying excited states were averaged with equal weight for the neutrals. The natural orbitals (NOs) obtained by the CASSCF method were used as one–particle functions in the CI calculations from the CAS reference space. All single and double excitations from the five active orbitals on Li and n ($2n$) high–lying occupied MOs corresponding to lone pairs in NH_3 (H_2O) molecules were included in the CI.

3 RESULTS AND DISCUSSION

3.1 Geometries and Total Binding Energies

3.1.1 $Li^-(NH_3)_n$ ($n = 1–4$)

Optimized geometries and $\Delta E(n)$ of $Li^-(NH_3)_n$ ($n = 1–4$) are shown in Figure 1. We use the labels of the form $p + q + r$ for each structure. The values of p, q and r are the numbers of solvent molecules bound by Li–N bonds, Li^-–H interaction and hydrogen bonding, respectively. We describe mainly $\Delta E(n)$ with both ZPC and CPC in the following text, and those with only ZPC are given in parentheses.

Two isomers were found for $n = 1$. One is A1a with a Li–N bond and another is A1b with Li^-–H interaction. The $\Delta E(1)$ of the former is 8.6(11.3) kcal/mol, which is larger than that of the latter by 5.8(8.2) kcal/mol. We examined five $n = 2$ clusters. A second NH_3 molecule is bound to A1a from N side, H side and by a hydrogen bond in A2a–c, respectively. The $\Delta E(2)$ of A2a is 19.8(25.5) kcal/mol. It is larger than those of A2b and A2c over 8.5(11.2) kcal/mol. Two other isomers (A2d and A2e) with no Li–N bond are further less stable. The similar energetic trend is seen for $n = 3$. A3a with three equivalent Li–N bonds is the most stable for this size. Its $\Delta E(3)$ is 32.1(41.0) kcal/mol. Three isomers (A3b–d) in which two NH_3 ligands are bound to Li by Li–N bonds and the third one is via Li^-–H or hydrogen–bond interaction are close in energy to one another, but they are less stable than A3a by about 10 kcal/mol. The other isomers with fewer Li–N bonds are further less stable. The incremental binding energies of the clusters with n Li–N bonds gradually increase as n grows. This energetic feature is related to the electronic states of these clusters as we will mention later. Since the most stable structure for each $n = 1 – 3$ tend to have as many Li–N bonds as possible, we optimized only three $n = 4$ complexes. One is A4a where all solvents are bound to the central Li from N sides, and two others are A4b and A4c in which a fourth NH_3 is bound to A3a via Li^-–H or hydrogen–bond interaction. The $\Delta E(4)$ of A4a is 42.0(53.7) kcal/mol.
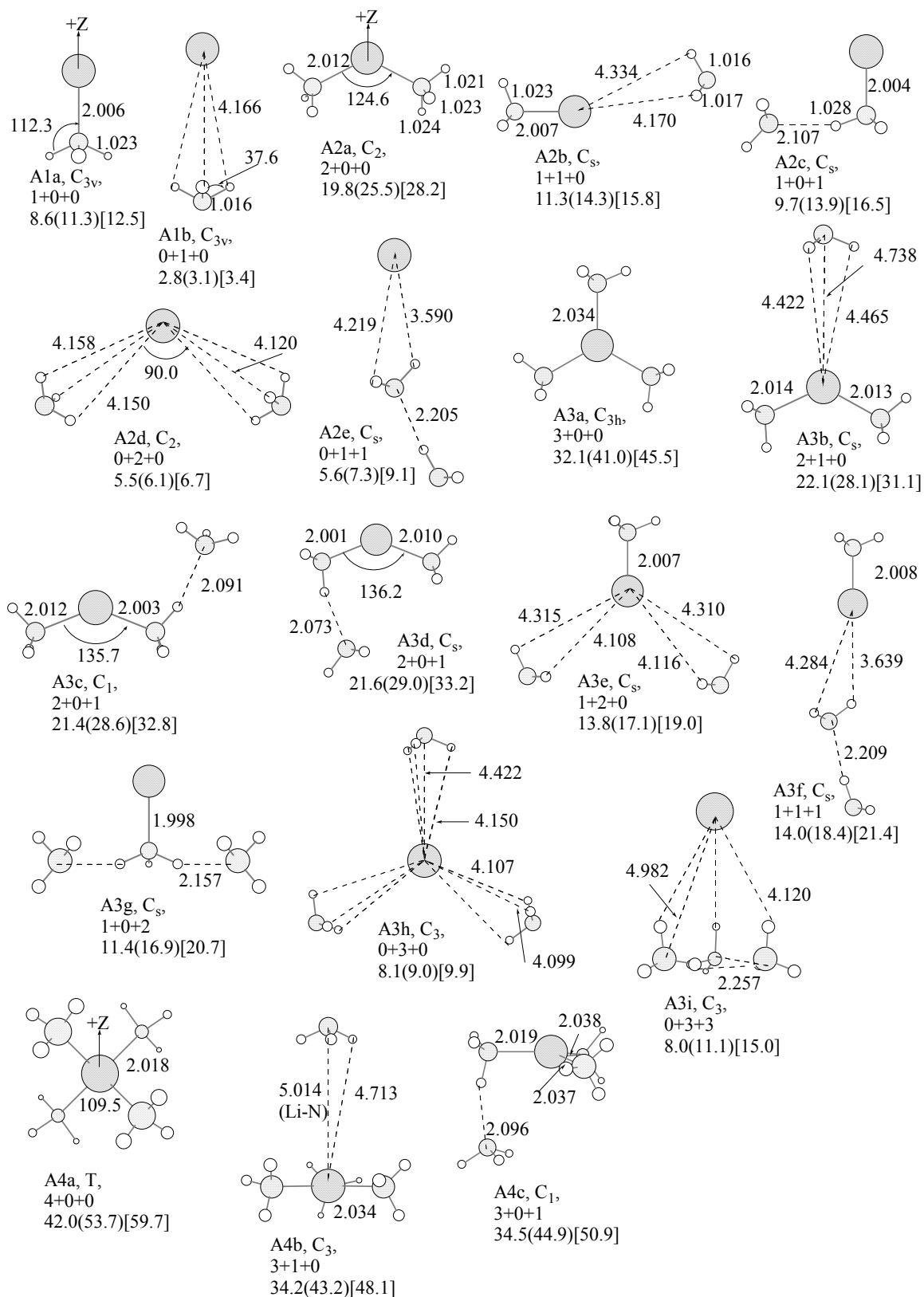
Figure 1. Structures of Li⁻(NH₃)ₙ (*n*=1–4). Geometrical parameters are given in Å and degrees. Total binding energies (kcal/mol) with both ZPC and CPC are presented under each structure. The values with only ZPC are in parentheses and those without ZPC and CPC are in brackets.

Though the energy difference between A4a and the second most stable A4b decreases from that between A3a and A3b for $n = 3$, the structure with four Li–N bonds is still much lower in energy than other isomers with three Li–N bonds. Thus, we conclude that the most stable forms of Li$^-$(NH$_3$)$_n$ for each $n = 1$–4 are the structures with the maximum numbers of Li–N bonds, being similar to the neutral and cationic Li (NH$_3$)$_n$ [30].

We have previously examined the geometries and $\Delta E(n)$ of Na$^-$(NH$_3$)$_n$ at the similar MP2 level with slightly larger basis sets [20]. The above structural characteristics of the most stable Li$^-$(NH$_3$)$_n$ for each n is similar to that of Na$^-$(NH$_3$)$_n$ though the Li–N lengths are shorter than Na–N bonds by around 0.4 Å in the clusters with the same n. On the other hand, the $\Delta E(1)$ for the A1a and A1b type Na$^-$(NH$_3$)$_1$ were 2.5(4.3) and 3.0(2.9) kcal/mol, respectively. The $\Delta E(1)$ values of Li$^-$(NH$_3$)$_1$ and Na$^-$(NH$_3$)$_1$ at the latter type geometries are close to each other because the electrostatic interaction governs the structures of both clusters and Na–H distances are longer than the Li–H lengths only by around 0.1 Å. The $\Delta E(1)$ of Li$^-$(NH$_3$)$_1$ at the former type configuration is about three times larger than the corresponding value of Na$^-$(NH$_3$)$_1$. The Li–N bond is much stronger than Na–N bond. As a result, the $\Delta E(4)$ of Li$^-$(NH$_3$)$_4$ having four metal–N bonds is larger than that of Na$^-$(NH$_3$)$_4$ by around 17(22) kcal/mol.

3.1.2 Li$^-$(H$_2$O)$_n$ ($n = 1$–4)

Optimized geometries and $\Delta E(n)$ of Li$^-$(H$_2$O)$_n$ ($n = 1$–4) are shown in Figure 2. The *p* value in the *p* + *q* + *r* type labels is the number of waters bound directly to Li by Li–O bonds in those structures. The $\Delta E(1)$ of W1a in which a water molecule is bound to Li from O side is 7.3(10.1) kcal/mol. This structure is more stable than W1b with Li$^-$–H interaction by 2.4(4.8) kcal/mol. The 2+0+0 structure (W2a) is the most stable for Li$^-$(H$_2$O)$_2$. Its $\Delta E(2)$ is 16.8(22.6) kcal/mol. The 1+1+0, 1+0+1 and 0+1+1 isomers (W2b–f) are as stable as one another but they all are less stable than W2a by more than 4.5 kcal/mol. Though we optimized the 0+2+0 isomer with D$_{2d}$ symmetry, it had degenerate imaginary frequencies. The further optimization following the imaginary normal mode reached W2e. For $n = 3$, the structure where all water molecules are bound by Li–O bonds is also the most stable, and the isomers with fewer Li–O bonds are higher in energy. The $\Delta E(3)$ of the 3+0+0 W3a is 27.8(37.0) kcal/mol, while those of the $p = 2$ complexes (W3b–d) are 21.6(27.9) – 20.7(29.4) kcal/mol. Neither the 1+2+0 C$_s$ structure nor the 0+3+0 D$_{3h}$ complex was a local–minimum. By following the imaginary normal modes, we finally obtained W3e–f from the former and W3i–l from the latter. The isomers with one or no Li–O bond is less stable than W3a by around 10–13 kcal/mol. Based on these results, we narrowed our focus mainly on the $n = 4$ clusters where four or three water molecules are bound to Li from O sides. Two 4+0+0 structures were found, whose $\Delta E(4)$ are 35.3(48.5) and 35.8(48.9) kcal/mol, respectively. They are so called interior structures, which are well known for the neutral and cationic states [14], and the $\Delta E(4)$ values depend only little on the orientations of water ligands. W4c in which the fourth water is bound to

W3a via hydrogen bond is less stable than W4a by 2.4(3.4) kcal/mol.
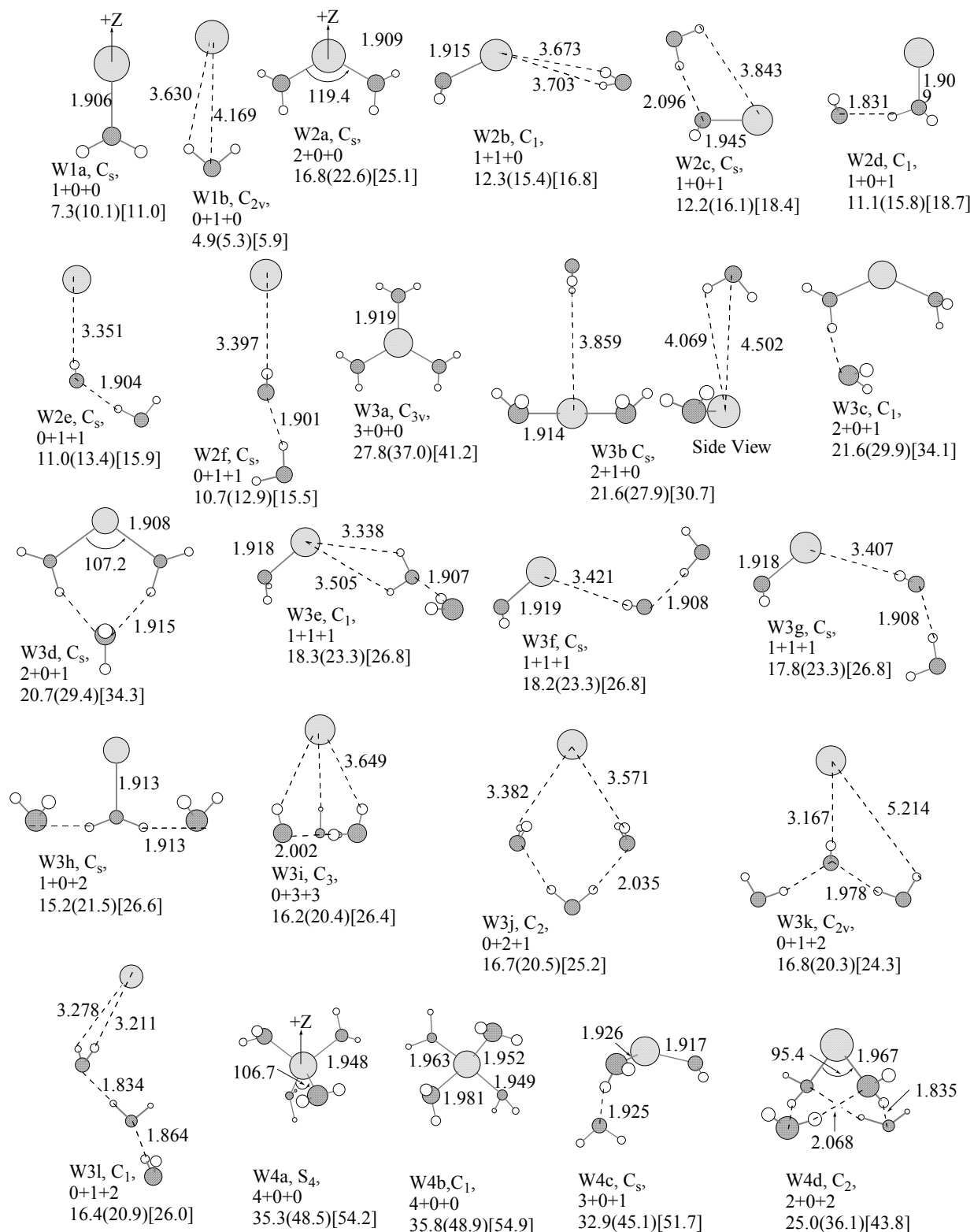
Figure 2. Structures of Li$^-$(H$_2$O)$_n$ (n = 1–4). Geometrical parameters are given in Å and degrees. Total binding energies (kcal/mol) with both ZPC and CPC are presented under each structure. The values with only ZPC are in parentheses and those without ZPC and CPC are in brackets.

The dependence of the $\Delta E(n)$ for $Li^-(H_2O)_n$ ($n = 1$–4) on the geometries is similar to that of Li^- $(NH_3)_n$. The most stable forms for each n have as many Li–nonhydrogen bonds as possible though the energy deviations between the most stable and the second most stable structures of $Li^-(H_2O)_n$ are smaller than the corresponding values of $Li^-(NH_3)_n$ with the same n. In the $n+0+0$ structures, the average Li–O and Li–N bond energies are 7.3(10.1)–9.3(12.3) kcal/mol and 8.6(11.3)–10.7(13.7) kcal/mol, respectively. The Li–N bond is a little stronger than Li–O bond. On the other hand, the Li^-–H interaction energy is by 2.1(2.2) kcal/mol larger in $Li^-(H_2O)_1$ than in $Li^-(NH_3)_1$. In addition, the hydrogen–bond energies estimated from the difference of the $\Delta E(n)$ between W1a and W2d and that between W1b and W2e are 3.8(5.7) and 6.1(8.1) kcal/mol, respectively. Though these numbers depend on the structures to some extent, both of them are also greater than corresponding energies in $Li^-(NH_3)_n$ (1.1(2.6) and 2.8(4.2) kcal/mol). Thus, the Li^-–H interaction and hydrogen–bond energies themselves are large in $Li^-(H_2O)_n$ relative to $Li^-(NH_3)_n$ but the formation of Li–O bonds even with avoiding the other two kinds of interactions is still a major contributor in stabilizing Li^- $(H_2O)_n$.

This structural and energetic feature of $Li^-(H_2O)_n$ is in marked contrast to $Na^-(H_2O)_n$ where Na^-–H and hydrogen bonds are important in dictating the low–energy structures for each n. For $Na^-(H_2O)_1$ anions, the $\Delta E(1)$ of W1a and W1b type forms were 3.8 and 4.9 kcal/mol without CPC, respectively, at the similar MP2 level with extended basis sets [21]. The hydrogen–bond energy calculated from the ΔE without CPC for W1b and W2e type $Na^-(H_2O)_{1,2}$ was 7.6 kcal/mol, which is close to that in $Li^-(H_2O)_2$. Therefore, the dissimilarity in the most stable forms between $Li^-(H_2O)_n$ and $Na^-(H_2O)_n$ with the same n results mainly from the strong Li–O bonds.

Since the hydrogen–bond energies in $Li^-(H_2O)_n$ are relatively large as mentioned above, one may expect that the so called surface structures where Li^- is situated on the surface of the cyclic hydrogen–bonded water clusters are the low–energy isomers for $n \geq 3$. However, the optimization searching for such $n = 3$ structure had reached W3a. On the other hand, we could find a surface W4d where two waters are in the first layer but it was much less stable than W4a. In the interior forms, the oxygen atoms are actually bound to the small Li^+ even in the negatively charged clusters as we will show later. The large binding energies are considered to result from the ionic nature of Li–O bonds.

3.2 Vertical Detachment Energies and Assignments of PES Bands

The calculated VDEs of $Li^-(NH_3)_n$ ($n = 0$–4) are summarized in Table 1 together with experimental values. We have previously examined the VDEs for the transition to the neutral ground state in A1a, A2a and A3a by the CCSD(T) method [19]. The present results at the MRSDCI level agree with the previous values within 0.05 eV.

Takasu *et al*. recorded the PESs for $Li^-(NH_3)_n$ by using the photodetachment energy of 3.50 eV

[6]. In their $n = 1$ spectrum, the first and second bands were observed at 0.56 and 2.05 eV, which are down–shifted from the atomic 2^2S– and 2^2P–type transitions by 0.06 and 0.42 eV, respectively. Another band was observed at 2.78 eV. In our calculations, the VDEs for the 2^2S– and 2^2P–type transitions in A1a are 0.39 and 1.80–1.92 eV, respectively, and their red shifts from $n = 0$ are in agreement with the experiment. The calculated VDE for the transition to the 3^2A_1 state in this isomer is 2.89 eV which is close to the experimental value of the third band. On the other hand, the VDEs for these transitions in A1b are 0.75, 2.59–2.63 and 4.16 eV. They are shifted to the blue from $n = 0$, which is opposite to the experimental observation. Thus, the three observed bands for $n = 1$ are assignable to the 2^2S– , 2^2P– and 3^2S–type transitions, respectively, in the structure with a Li–N bond. Though the calculations show that the transitions to 2^2P–like states are expected to split upon complex formation, it is difficult to argue the splitting due to the low spectral resolution.

Table 1. Vertical detachment energies (eV) for transitions from anionic ground state to neutral ground and low–lying excited states of $Li(NH_3)_n$ ($n \le 4$)[a] at MRSDCI level together with experimental values.[b,c]

$n = 0$			$n = 1$						$n = 2$		
Expt.	Li Atom[d]		Expt.	A1a		A1b			Expt.	A2a	
	0+0+0			1+0+0		0+1+0				2+0+0	
0.62	2^2S	0.61	0.56	1^2A_1	0.39	1^2A_1	0.75		0.56	1^2A	0.38
					(0.44)						(0.43)
2.47	2^2P	2.45	2.05	1^2E	1.80	1^2E	2.59		~1.5	2^2A	1.31
				2^2A_1	1.92	2^2A_1	2.63			1^2B	1.36
										2^2B	1.40
	3^2S	3.96	2.78	3^2A_1	2.89	3^2A_1	4.16		~2	3^2A	2.19

$n = 2$									$n = 3$		
A2b		A2c		A2d		A2e			Expt.	A3a	
1+1+0		1+0+1		0+2+0		0+1+1				3+0+0	
$1^2A'$	0.48	$1^2A'$	0.24	1^2A	0.88	$1^2A'$	0.84		0.50	$1^2A'$	0.40
											(0.44)
$2^2A'$	1.91	$2^2A'$	1.63	1^2B	2.72	$2^2A'$	2.69		1.41	$1^2E'$	1.10
$1^2A''$	1.91	$1^2A''$	1.63	2^2A	2.75	$1^2A''$	2.70				
$3^2A'$	2.10	$3^2A'$	1.95	2^2B	2.78	$3^2A'$	2.73			$1^2A''$	1.14
$4^2A'$	3.10	$4^2A'$	2.58	3^2A	4.38	$4^2A'$	4.30		2.30	$2^2A'$	2.01

$n = 3$									$n = 4$		
A3b		A3c		A3e		A3h			Expt.	A4a	
2+1+0		2+0+1		1+2+0		0+3+0				4+0+0	
$1^2A'$	0.45	1^2A	0.28	$1^2A'$	0.57	1^2A	1.02		0.43	1^2A	0.40
$2^2A'$	1.44	2^2A	1.15	$1^2A''$	2.00	2^2A	2.85		1.32	1^2T	1.01
$1^2A''$	1.45	3^2A	1.18	$2^2A'$	2.07	1^2E	2.91				
$3^2A'$	1.50	4^2A	1.33	$3^2A'$	2.22						
$4^2A'$	2.32	5^2A	1.87	$4^2A'$	3.29	3^2A	4.59		2.21	2^2A	1.93

[a] Structures are given in Figure 1. [b] Experimental values are from Ref. [6]. [c] Values in parentheses are by CCSD(T) from Ref. [19]. [d] With no frozen core.

For $n = 2$, two bands were observed at 0.56 and ~1.5 eV, and a weak broad band was at ~2 eV. The position of the first band is almost unchanged from $n = 1$, while those of the higher bands are shifted to the lower EBE by ~0.6 and ~0.8 eV, respectively. In A2a, the VDE for the 2^2S–type

transition is very close to that of A1a, and those for the 2^2P– and 3^2S–type transitions decrease by ~0.5 and ~0.7 eV, respectively, from the corresponding values for A1a. On the other hand, the VDEs of A2b increase by ~0.1 eV from those of the same type transitions in A1a. In addition, the changes of VDEs from A1a to the other higher–energy $n = 2$ isomers do not match the observed spectral shifts from $n = 1$ to $n = 2$. Thus, the observed bands for $n = 2$ can be assigned to the 2^2S–, 2^2P– and 3^2S–type transitions, respectively, in the 2+0+0 complex.

For $n = 3$, we list the VDEs for three lowest–energy structures and two representative high–energy isomers with one or no Li–N bonds in the table for brevity. The photoelectron bands for $n = 3$ were observed at 0.50, 1.41 and 2.30 eV, while those for $n = 4$ were at 0.43, 1.32 and 2.21 eV. The near constancy of the first band and the red shifts of the higher bands with increasing n are best reproduced by A3a among the $n = 3$ complexes and A4a also reproduces these spectral features well. Thus, we can assign the PES bands for $n = 3$ and 4 to the 2^2S–, 2^2P– and 3^2S–type transitions in A3a and A4a, respectively. The first bands for $n = 2$ and 3 have a shoulder at ca. 0.9–1.0 eV. The transition to the neutral ground state in the higher–energy isomers such as A2d and A3h, where all NH_3 molecules are bound to Li⁻ from H sides, may correspond to the shoulder peaks. However, their separations from the main peak and the absence of other isomer–bands seem to suggest the vibrational transition of NH stretch in the structures with n Li–N bonds though further effort is necessary to assign the shoulder peaks definitely.

For all n examined, the second and third bands can be attributed not to the local–minimum isomers but to the transitions to the low–lying excited states in the most stable forms for each n. The structures in which all NH_3 molecules are bound directly to Li by Li–N bonds are responsible for the observed PESs for $n = 1 – 4$. In these isomers, the VDEs for the transition to the neutral ground state are almost constant and those to the excited states decrease rapidly as n grows. The former has been ascribed to the close solvation energies of the anionic and neutral ground states at these geometries [19], while the latter will be discussed in detail in the later section. On the other hand, when an NH_3 molecule is bound to the clusters from H side, the VDEs to the ground and low–lying excited states of the neutrals increase roughly in parallel with one another as we see in the changes of VDEs from A1a to A2b for example. It is natural because the binding energies at these anion geometries are gained by the electrostatic interaction between Li⁻ and positive charges on H atoms which is absent in the neutrals. The VDEs to both ground and low–lying excited states for the 0+n+0 structures increase monotonically as n grows by keeping their separation nearly constant, which is similar to the observed size dependence of the PESs for Na⁻$(H_2O)_n$.

The calculated VDEs of Li⁻$(H_2O)_n$ ($n = 1–4$) are listed in Table 2 together with experimental values. Though Takasu et al. examined the PESs of Li⁻$(D_2O)_n$ to improve the mass separation of Li⁻–water clusters and the reaction products such as $LiO^-(H_2O)_n$, the PESs of Li⁻$(H_2O)_n$ should be essentially the same [18]. The first PES bands were observed at 0.56 ($n = 1$), 0.57 ($n = 2$), 0.56 ($n =$

3) and 0.53 ($n = 4$) eV, respectively, while the second bands were at 1.97 ($n = 1$), 1.72 ($n = 2$), 1.50 ($n = 3$) and 1.45 ($n = 4$) eV.

Table 2. Vertical detachment energies (eV) for transitions from anionic ground state to neutral ground and low–lying excited states of Li(H$_2$O)$_n$ ($n \leq 4$)[a] at MRSDCI level together with experimental values.[b,c]

	$n = 1$					$n = 2$			
Expt.	W1a		W1b		Expt.	W2a		W2b	
	1+0+0		0+1+0			2+0+0		1+1+0	
0.56	1^{2}A′	0.47	1^{2}A$_1$	0.87	0.57	1^{2}A′	0.46	1^{2}A	0.64
		(0.51)					(0.50)		
1.97	2^{2}A′	1.92	2^{2}A$_1$	2.72	1.72	2^{2}A′	1.51	2^{2}A	2.25
	1^{2}A″	1.97	1^{2}B$_1$	2.75		1^{2}A″	1.65	3^{2}A	2.29
	3^{2}A′	2.20	2^{2}B$_2$	2.80		3^{2}A′	1.94	4^{2}A	2.53
	4^{2}A′	3.15	3^{2}A$_1$	4.47		4^{2}A′	2.59	5^{2}A	3.68

	$n = 2$					$n = 3$					
W2c		W2d		W2e		Expt.	W3a		W3b		W3c
1+0+1		1+0+1		0+1+1			3+0+0		2+1+0		2+0+1
1^{2}A′ 0.64		1^{2}A 0.40		1^{2}A′ 1.08		0.56	1^{2}A$_1$ 0.46		1^{2}A′ 0.61		1^{2}A 0.46
							(0.51)				
2^{2}A′ 2.12		2^{2}A 1.84		2^{2}A′ 2.97		1.50	1^{2}E 1.37		2^{2}A′ 1.78		2^{2}A 1.39
1^{2}A″ 2.21		3^{2}A 1.96		1^{2}A″ 3.00					1^{2}A″ 2.02		3^{2}A 1.72
3^{2}A′ 2.46		4^{2}A 2.34		3^{2}A′ 3.06			2^{2}A$_1$ 1.90		3^{2}A′ 2.28		4^{2}A 1.90
4^{2}A′ 3.55		5^{2}A 3.00		4^{2}A′ 4.83			3^{2}A$_1$ 2.39		4^{2}A′ 3.05		5^{2}A 2.54

	$n = 3$					$n = 4$					
W3e		W3h		W3l		Expt.	W4a		W4b		W4c
1+1+1		1+0+2		0+1+2			4+0+0		4+0+0		3+0+1
1^{2}A 0.23		1^{2}A′ 0.46		1^{2}A 1.25		0.53	1^{2}A 0.44		1^{2}A 0.38		1^{2}A′ 0.35
2^{2}A 1.90		1^{2}A″ 1.93		2^{2}A 3.19		1.45	2^{2}A 1.02		2^{2}A 1.21		2^{2}A′ 1.37
3^{2}A 1.96		2^{2}A′ 2.00		3^{2}A 3.17			1^{2}E 1.27		3^{2}A 1.38		1^{2}A″ 1.41
4^{2}A 2.26		3^{2}A′ 2.72		4^{2}A 3.25					4^{2}A 1.55		3^{2}A′ 1.71
5^{2}A 3.41		4^{2}A′ 3.11		5^{2}A 5.08			3^{2}A 2.11		5^{2}A 2.20		4^{2}A′ 2.22

[a] Structures are given in Figure 2. [b] Experimental values are from Ref. [18]. [c] Values in parentheses are by CCSD(T) from Ref. [19]

The VDEs for the transition to the neutral ground state in W1a, W2a and W3a by the present MRSDCI method deviate at most 0.05 eV from the previous results at the CCSD(T) level [19]. For Li$^-$(H$_2$O)$_1$, the calculated VDEs for the 2^{2}S–, 2^{2}P– and 3^{2}S–type transitions in W1a are 0.47, 1.92–2.20 and 3.15 eV, respectively. The decreases of the VDEs for the transitions to the 2^{2}S– and 2^{2}P–like states from $n = 0$ reproduce well the observed spectral shifts. On the other hand, in W1b, the VDE for the transition to the neutral ground state increases from the corresponding atomic value and those to the excited states do as well. Thus, we can assign the first and second observed bands to the 2^{2}S– and 2^{2}P–type transitions in W1a with a Li–O bond.

For $n \geq 1$, both near constancy of the VDEs for the first bands and the rapid decrease of the VDEs for the second bands are well reproduced by the calculated values for the 2^{2}S– and 2^{2}P–type transitions in the most stable structures for each n. The VDEs of W4a and W4b, in which all four water molecules are bound directly to Li from O sides with different orientations, are close to each

other. Thus, on the basis of the size dependence of the PES bands, we can assign the first and second PES bands to the 2^2S- and 2^2P-type transitions in the structures with n Li–O bonds for $n = 1 – 4$ rather than the isomer–bands, though the present calculations tend to underestimate the absolute VDEs by ~0.2 eV.

On the other hand, the VDEs for the transitions to each neutral state in W1b, W2e and W3l, whose structures resemble the most stable Na$^-$(H$_2$O)$_n$ for $n = 1$–3, respectively, increase with n. This behavior of the VDEs is similar to the size dependence of the VDEs for the observed PES bands for Na$^-$(H$_2$O)$_n$ though these structures are high–energy isomers of Li$^-$(H$_2$O)$_n$ for each n. The remarkable metal dependence of the PES bands between Li$^-$(H$_2$O)$_n$ and Na$^-$(H$_2$O)$_n$ results from the difference of their most stable structures for each n.

3.3 Electronic Nature

3.3.1 Anionic and neutral ground states

We examined the electronic nature of anionic and neutral ground states of the solvation clusters in terms of the radial distribution functions, $\rho(r)$, of the valence electrons. We used the highest doubly (DOMO) or singly occupied molecular orbital (SOMO) by the Hartree–Fock method with Li at the origin.

$$\rho(r) = \int_{0(\theta)}^{\pi} \int_{0(\varphi)}^{2\pi} \left| \phi_i \right|^2 r^2 \sin\theta d\varphi d\theta \quad (\phi_i = \text{DOMO or SOMO}).$$ (2)

We divided the function into two components, $\rho_+(r)$ and $\rho_-(r)$, which were contributions from half spheres with $z \geq 0$ and with $z < 0$, respectively. The molecular symmetry axis was taken as the z–axis and the direction with positive z values for $n = 1, 2$ and 4 clusters are shown in Figures 1 and 2. We examined the high symmetry W4a because the electronic nature of Li(H$_2$O)$_4$ is expected to depend little on the water orientation. The positive z direction for the C$_{3v}$ W3a is the direction in which hydrogen atoms do not exist. The sum of $\rho_+(r)$ and $\rho_-(r)$ gives the total function $\rho(r)$.

$$\rho(r) = \rho_+(r) + \rho_-(r).$$ (3)

We have also evaluated the number of electrons distributed inside the half spheres with a radius of r, $N_+(r)$ and $N_-(r)$, by integrating the $\rho_+(r)$ and $\rho_-(r)$, respectively.

$$N_\pm(r) = \int_0^r n\rho_\pm(r')dr' \quad (n = 2 \text{ (DOMO) or 1 (SOMO))}.$$ (4)

The $\rho_+(r)$, $\rho_-(r)$, $N_+(r)$ and $N_-(r)$ for Li(NH$_3$)$_n$ and Li(H$_2$O)$_n$ are presented in Figures 3–6. The peak positions and the maximum values of the $\rho_+(r)$ and $\rho_-(r)$ are summarized in Table 3. The $N_+(r)$ and $N_-(r)$ at r only slightly shorter than the Li–N (Li–O) lengths, say r_{Li-N} (r_{Li-O}), and those at another r which is little longer than the distance between Li and outermost H atom (r_{Li-H}) are listed in Table 4.
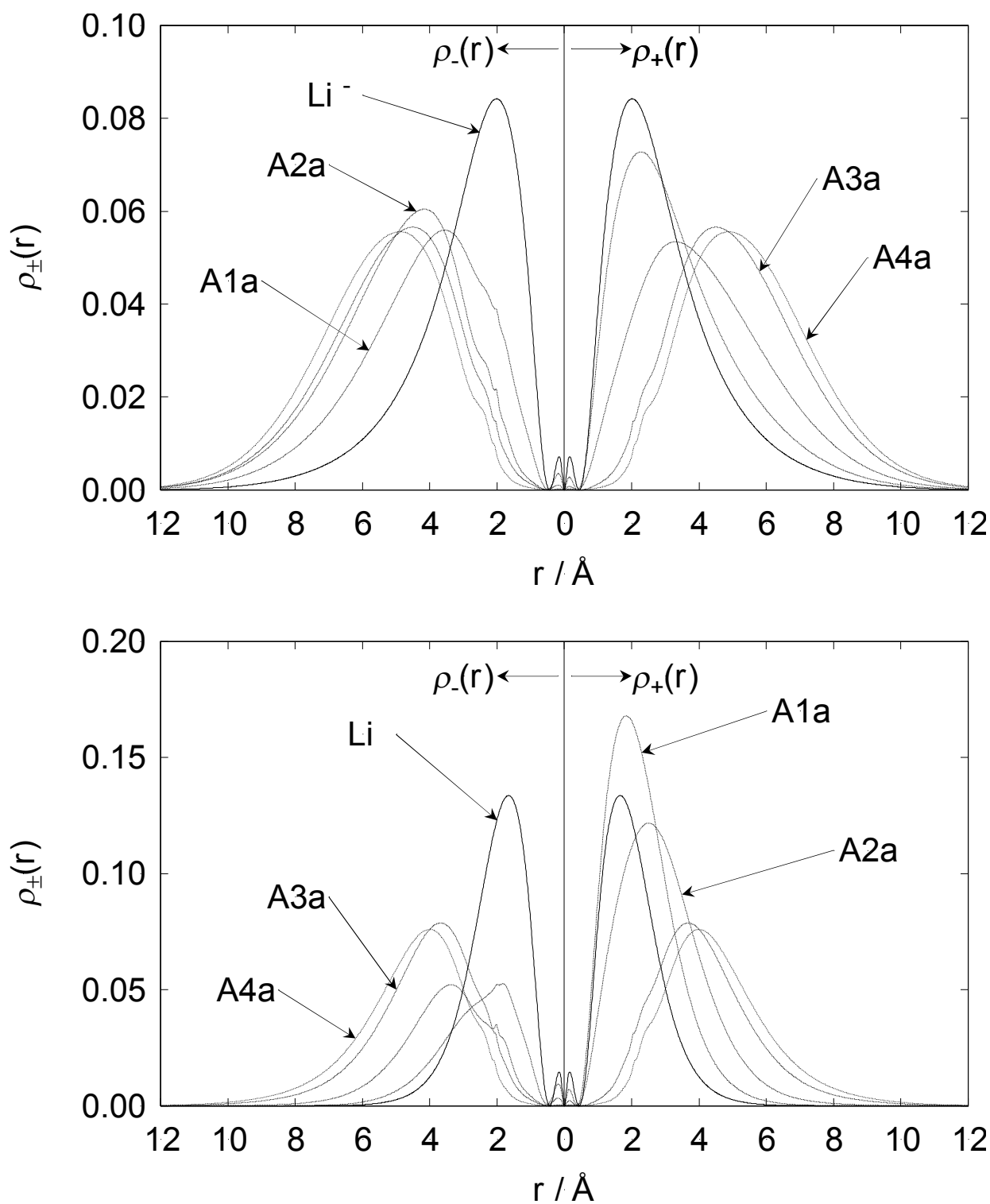
Figure 3. Contribution of a half sphere with $z \geq 0$ ($\rho_+(r)$) and that with $z < 0$ ($\rho_-(r)$) to radial distribution function of valence electrons derived from Li for Li$^-$(NH$_3$)$_n$ (upper panel) and Li(NH$_3$)$_n$ (lower panel) ($n = 0$–4). Li is at the origin.
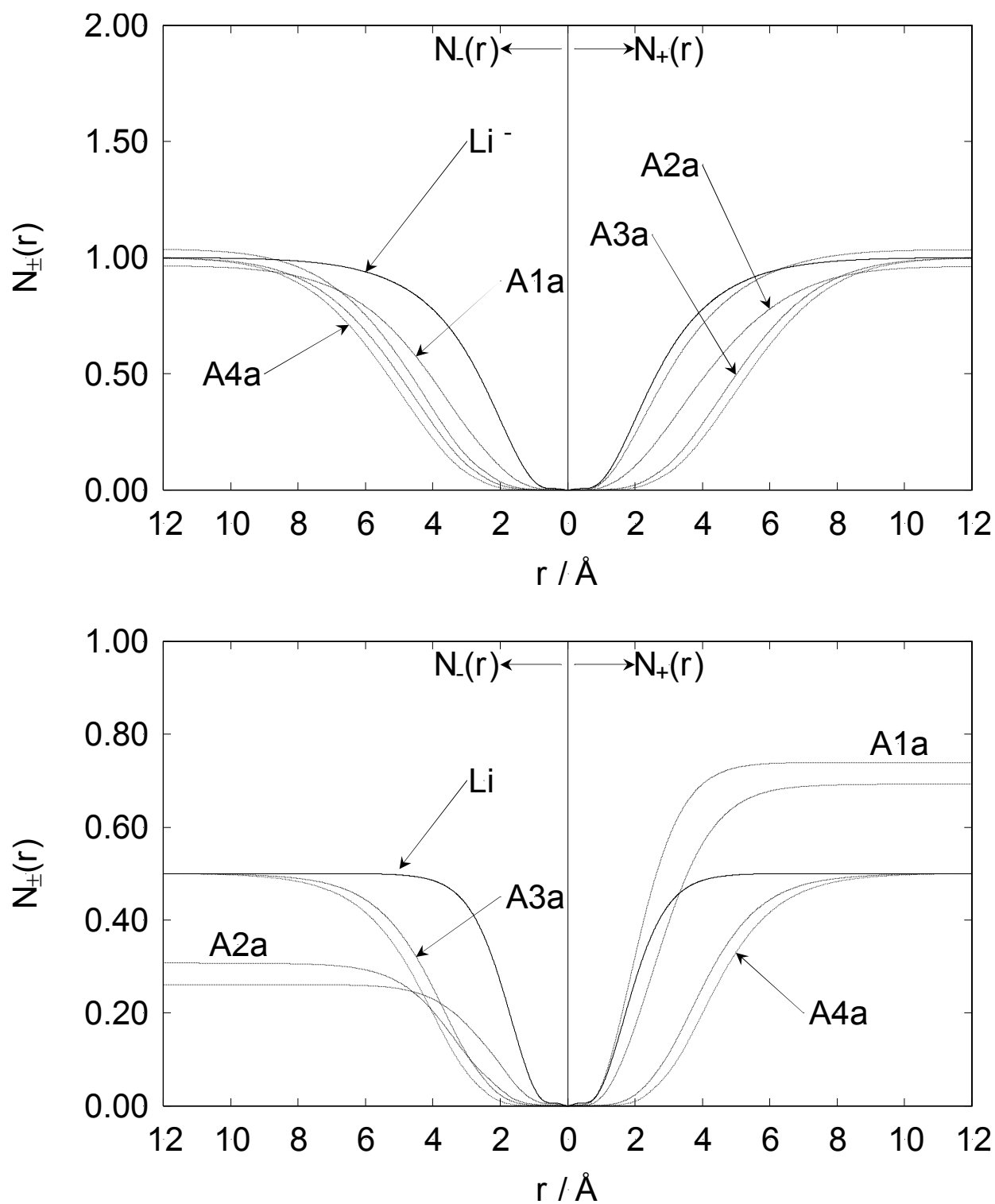
Figure 4. Number of valence electrons derived from Li distributed inside the half spheres with a radius of *r*, $N_+(r)$ and $N_-(r)$ for $Li^-(NH_3)_n$ (upper panel) and $Li(NH_3)_n$ (lower panel) (*n* = 0–4).
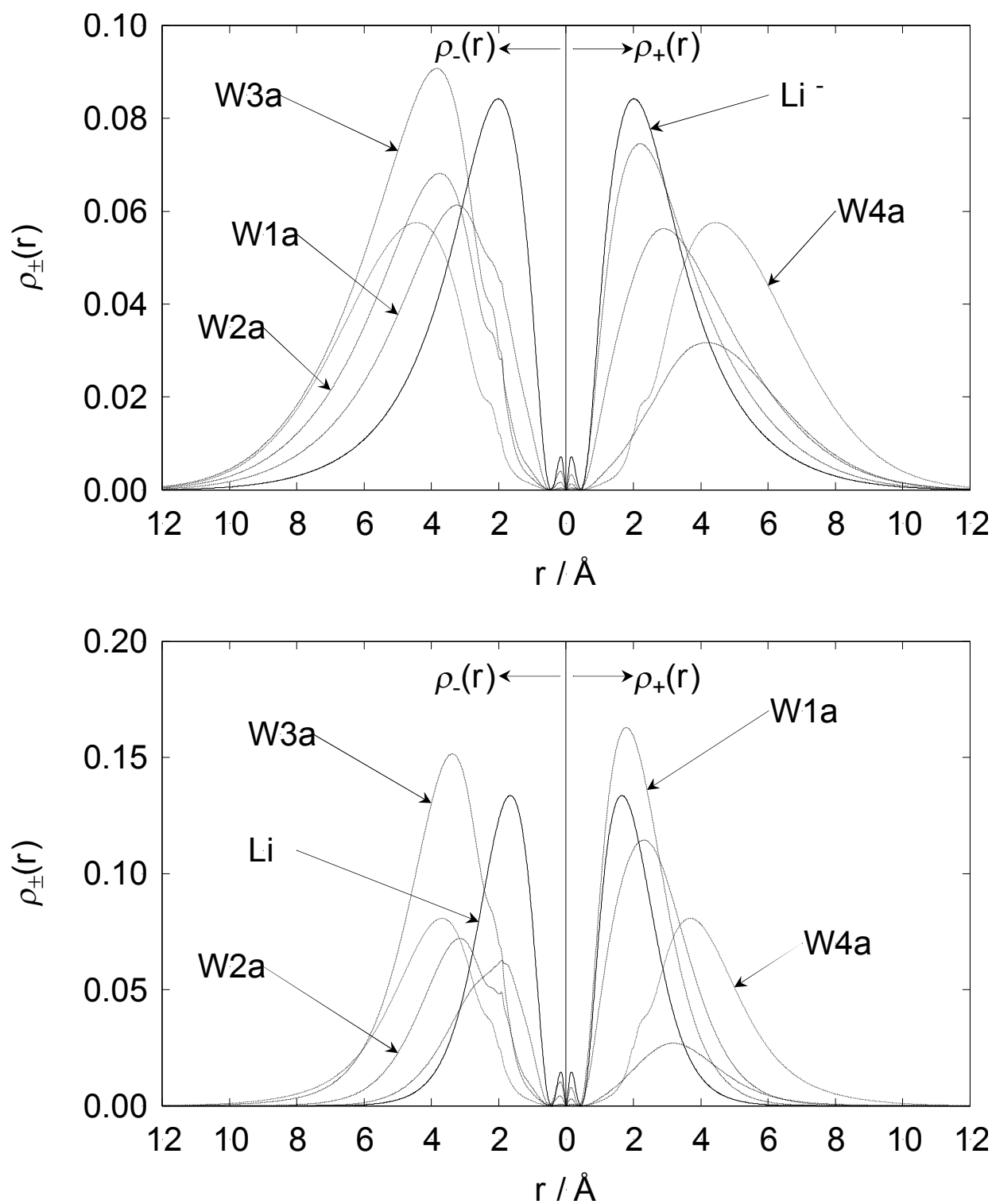
Figure 5. Contribution of a half sphere with $z \geq 0$ ($\rho_+(r)$) and that with $z < 0$ ($\rho_-(r)$) to radial distribution function of valence electrons derived from Li for $Li^-(H_2O)_n$ (upper panel) and $Li(H_2O)_n$ (lower panel) ($n = 0$–4). Li is at the origin.
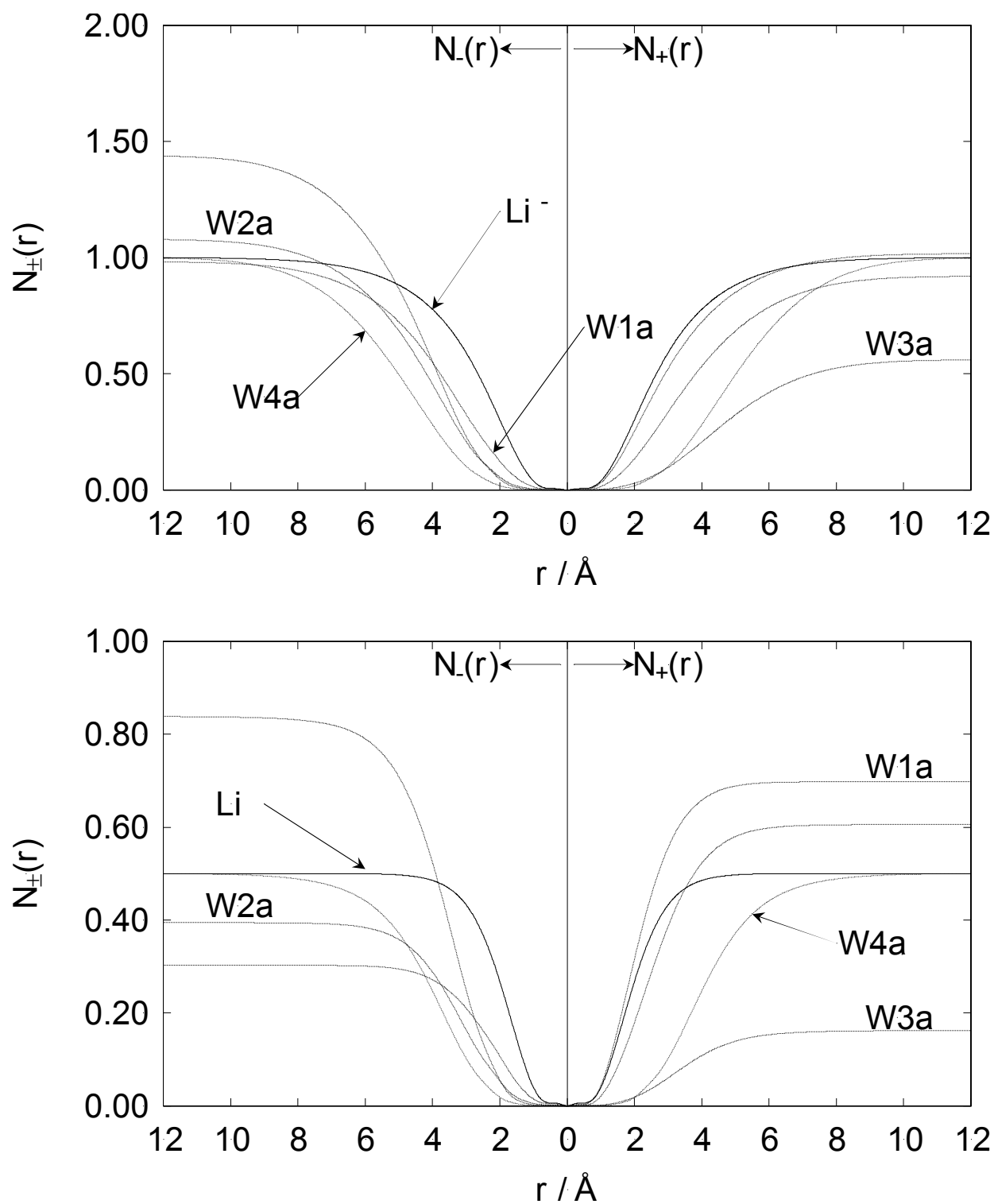
Figure 6. Number of valence electrons derived from Li distributed inside the half spheres with a radius of *r*, $N_+(r)$ and $N_-(r)$ for Li⁻(H₂O)ₙ (upper panel) and Li(H₂O)ₙ (lower panel) (*n* = 0–4).

Table 3. Peak position (Å) and maximum value of $\rho(r)$ and its components.

			Li⁻(NH₃)ₙ							Li⁻(H₂O)ₙ			
label	$r_{\rho-max}$	$\rho_-(r)$	$r_{\rho+max}$	$\rho_+(r)$	$r_{\rho max}$	$\rho(r)$	label	$r_{\rho-max}$	$\rho_-(r)$	$r_{\rho+max}$	$\rho_+(r)$	$r_{\rho max}$	$\rho(r)$
Li	2.01	0.084	2.01	0.084	2.01	0.168							
A1a	3.56	0.056	2.27	0.073	2.82	0.117	**W1a**	3.24	0.061	2.20	0.075	2.73	0.126
A2a	4.16	0.060	3.30	0.053	3.89	0.111	**W2a**	3.75	0.068	2.90	0.056	3.49	0.120
A3a	4.50	0.057	4.50	0.057	4.50	0.113	**W3a**	3.84	0.091	4.18	0.032	3.90	0.122
A4a	4.89	0.056	4.89	0.056	4.89	0.111	**W4a**	4.43	0.058	4.43	0.058	4.43	0.115

			Li(NH₃)ₙ							Li(H₂O)ₙ			
label	$r_{\rho-max}$	$\rho_-(r)$	$r_{\rho+max}$	$\rho_+(r)$	$r_{\rho max}$	$\rho(r)$	label	$r_{\rho-max}$	$\rho_-(r)$	$r_{\rho+max}$	$\rho_+(r)$	$r_{\rho max}$	$\rho(r)$
Li	1.66	0.134	1.66	0.134	1.66	0.267							
A1a	1.84	0.168	1.83	0.053	1.83	0.220	**W1a**	1.91	0.063	1.79	0.163	1.89	0.224
A2a	3.37	0.052	2.51	0.122	2.82	0.162	**W2a**	3.16	0.072	2.31	0.114	2.76	0.172
A3a	3.68	0.079	3.68	0.079	3.68	0.157	**W3a**	3.38	0.152	3.18	0.027	3.36	0.178
A4a	4.00	0.076	4.00	0.076	4.00	0.152	**W4a**	3.69	0.081	3.69	0.081	3.69	0.161

Table 4. $N_-(r)$, $N_+(r)$ and their sum, $N(r)$, at r_{Li-N}, r_{Li-O}, r_{Li-H} (Å) and at infinite separation from Li.

		Li⁻(NH₃)ₙ			Li(NH₃)ₙ					Li⁻(H₂O)ₙ			Li(H₂O)ₙ		
		A1a			**A1a**					**W1a**			**W1a**		
	r	$N_-(r)$	$N_+(r)$	$N(r)$	$N_-(r)$	$N_+(r)$	$N(r)$		r	$N_-(r)$	$N_+(r)$	$N(r)$	$N_-(r)$	$N_+(r)$	$N(r)$
N	2.00	0.100	0.240	0.340	0.089	0.321	0.410	O	1.90	0.107	0.225	0.331	0.095	0.286	0.381
H	2.57	0.190	0.395	0.586	0.141	0.484	0.625	H	2.47	0.211	0.384	0.595	0.159	0.446	0.605
	∞	0.965	1.035	2.000	0.261	0.739	1.000		∞	0.983	1.017	2.000	0.302	0.698	1.000
		A2a			**A2a**					**W2a**			**W2a**		
	r	$N_-(r)$	$N_+(r)$	$N(r)$	$N_-(r)$	$N_+(r)$	$N(r)$		r	$N_-(r)$	$N_+(r)$	$N(r)$	$N_-(r)$	$N_+(r)$	$N(r)$
N	2.01	0.036	0.104	0.141	0.037	0.173	0.209	O	1.90	0.044	0.117	0.162	0.044	0.158	0.203
H	2.59	0.093	0.199	0.292	0.075	0.303	0.378	H	2.48	0.116	0.225	0.341	0.100	0.282	0.382
	∞	1.038	0.962	2.000	0.307	0.693	1.000		∞	1.080	0.920	2.000	0.394	0.606	1.000
		A3a			**A3a**					**W3a**			**W3a**		
	r	$N_-(r)$	$N_+(r)$	$N(r)$	$N_-(r)$	$N_+(r)$	$N(r)$		r	$N_-(r)$	$N_+(r)$	$N(r)$	$N_-(r)$	$N_+(r)$	$N(r)$
N	2.03	0.023	0.023	0.046	0.025	0.025	0.050	O	1.91	0.036	0.025	0.061	0.044	0.016	0.059
H	2.61	0.067	0.067	0.134	0.070	0.070	0.139	H	2.50	0.121	0.057	0.177	0.135	0.037	0.172
	∞	1.000	1.000	2.000	0.500	0.500	1.000		∞	1.440	0.560	2.000	0.838	0.162	1.000
		A4a			**A4a**					**W4a**			**W4a**		
	r	$N_-(r)$	$N_+(r)$	$N(r)$	$N_-(r)$	$N_+(r)$	$N(r)$		r	$N_-(r)$	$N_+(r)$	$N(r)$	$N_-(r)$	$N_+(r)$	$N(r)$
N	2.08	0.012	0.012	0.024	0.012	0.012	0.024	O	1.94	0.015	0.015	0.030	0.016	0.016	0.031
H	2.64	0.044	0.044	0.088	0.043	0.043	0.086	H	2.59	0.058	0.058	0.117	0.059	0.059	0.118
	∞	1.000	1.000	2.000	0.500	0.500	1.000		∞	1.000	1.000	2.000	0.500	0.500	1.000

As seen in the upper panel of Figure 3, the peaks of both $\rho_+(r)$ and $\rho_-(r)$ for bare Li⁻ are at 2.01 Å, and they are shifted to the longer r as the number of NH_3 molecules increases. The spatial expansion of the valence electron distribution occurs in Li⁻(NH₃)ₙ with increasing n. For $n \leq 2$, the $\rho_+(r)$ is peaked at shorter r than that of $\rho_-(r)$, and $N_+(r)$ rises faster than $N_-(r)$. On the other hand, the $\rho_+(r)$ and $\rho_-(r)$ for larger n become symmetric, and both $N_+(r)$ and $N_-(r)$ for all n converge to (nearly) one. Though NH_3 molecules push the valence electrons to the space in the direction free

from the solvents in the small r region in the $n \leq 2$ anions, the valence electron distribution is essentially diffuse in all these cluster anions. Note that the peak of $\rho_-(r)$ for even $Li^-(NH_3)_1$ is at 3.56 Å which is longer than r_{Li-H} (2.674 Å). Interestingly, the sum of $N_+(r)$ and $N_-(r)$, which we designate $N(r)$ from now, at r_{Li-N} and that at r_{Li-H} are 0.046 and 0.134, respectively, in A3a (see Table 4). The corresponding values in A4a are 0.024 and 0.088, respectively. Thus, more than 85 percents of the valence electrons are distributed outside the solvents in these structures. Namely, even in the negatively charged $Li^-(NH_3)_n$ ($n \geq 3$), $Li^+(NH_3)_n$ cationic core is surrounded by the diffused electrons. The spatial expansion of the valence electron distribution with increasing n also occurs in the neutrals as we see in the lower panel of Figure 3. Of course, both $\rho_+(r)$ and $\rho_-(r)$ are peaked at short r compared to the corresponding functions of the anions with the same n as one would expect. The $N_+(r)$ and $N_-(r)$ in neutral A1a and A2a are asymmetric with the former converging to 0.739 (A1a) and 0.693 (A2a), while these functions for $n \geq 3$ are symmetric reflecting their structures. The unpaired electron is polarized in the $n \leq 2$ neutrals. The $N(r)$ at r_{Li-H} in the neutral A3a and A4a are 0.139 and 0.086, respectively, as we see in Table 4. Most unpaired electrons are squeezed out of the solvation shell in the $n \geq 3$ neutrals.

The electronic change of anionic and neutral Li with stepwise hydration is qualitatively the same as that in Li–ammonia systems. The peak positions of $\rho_+(r)$ and $\rho_-(r)$ are shifted to the longer r with increasing n in both anionic and neutral states. The valence electrons are separated from Li^+ as n grows. The $N(r)$ values in Table 3 indicate that ~80 to ~90 percents of the valence electrons are distributed outside the outermost H atoms in the anionic and neutral $n \geq 3$ clusters. The water molecules are actually bound to Li^+ even in the anionic state for these n, and $Li^+(H_2O)_n$ core is surrounded by the diffused electron(s), which results in the strong ionic Li–O bonds.

Additionally, we can notice the interesting asymmetric behavior of $N_+(r)$ and $N_-(r)$ for $n = 3$. In W3a, all H atoms are in negative z side. Three dimensional contour plot of DOMO (not shown for brevity) for the anion shows that the electron cloud for relatively high value (0.02 e $Bohr^{-3/2}$) is near hydrogen atoms, while that of SOMO for the neutral indicates that the cloud is mainly expanded in the space outside hydrogen atoms in the negative z direction. The H atoms play a role in localizing the electrons to some extent in these clusters.

3.3.2 Neutral excited states

Expectation values of the radial distribution function for the unpaired electron (RD) in each neutral state were evaluated by the square root of the diagonal sum of the orbital component of the second moment for the CI–NO whose occupation number was nearly one (>0.99). They were calculated with Li at the origin. The results are given in Tables 5 and 6.

The RD values for the ground–state A1a, A2a A3a and A4a increase as n grows, which is consistent with the discussion in the previous section. The RDs for their excited states also become

large with increasing n. The RDs for the 1^2A and 1^2T states in A4a are about double the corresponding atomic values. The unpaired electron distribution for the $3^2S(Li)$ state is diffuse even without solvents. It is further diffused gradually from $n = 0$ to $n = 4$. The spatial expansion of the unpaired electron by the solvation occurs not only in the ground state but also in the low–lying excited states. The growing one–center (Rydberg–like) ion pair nature gives rise to the successive decrease of the energy separations between the ground and the low–lying excited states. As a result, the second and third PES bands for the transitions to the 2^2P– and 3^2S–like states are red–shifted with increasing n.

Table 5. Expectation values of radial distribution for unpaired electron (RD, Å) in each neutral state at anionic geometries of Li(NH$_3$)$_n$ ($n \leq 4$).[a] Li is at the origin.

$n = 0$		$n = 1$				$n = 2$			
Li Atom		A1a		A1b		A2a		A2b	
0+0+0		1+0+0		0+1+0		2+0+0		1+1+0	
2^2S	2.23	1^2A_1	2.63	1^2A_1	2.23	1^2A	3.43	$1^2A'$	2.60
2^2P	2.78	1^2E	3.41	1^2E	2.76	2^2A	4.60	$2^2A'$	3.34
						1^2B	4.36	$1^2A''$	3.34
		2^2A_1	4.36	2^2A_1	2.74	2^2B	5.05	$3^2A'$	4.35
3^2S	5.91	3^2A_1	6.36	3^2A_1	5.85	3^2A	6.53	$4^2A'$	6.33

$n = 2$						$n = 3$			
A2c		A2d		A2e		A3a		A3b	
1+0+1		0+2+0		0+1+1		3+0+0		2+1+0	
$1^2A'$	2.65	1^2A	2.22	$1^2A'$	2.22	$1^2A'$	4.27	$1^2A'$	3.35
$2^2A'$	3.64	1^2B	2.74	$2^2A'$	2.74	$1^2E'$	5.48	$2^2A'$	4.59
$1^2A''$	3.56	2^2A	2.73	$1^2A''$	2.74			$1^2A''$	4.22
$3^2A'$	4.90	2^2B	2.71	$3^2A'$	2.73	$1^2A''$	5.20	$3^2A'$	4.94
$4^2A'$	6.36	3^2A	5.77	$4^2A'$	5.78	$2^2A'$	6.79	$4^2A'$	6.47

$n = 3$						$n = 4$	
A3c		A3e		A3h		A4a	
2+0+1		1+2+0		0+3+0		4+0+0	
1^2A	3.58	$1^2A'$	2.58	1^2A	2.22	1^2A	4.65
2^2A	4.91	$1^2A''$	3.27	2^2A	2.71	1^2T	5.80
3^2A	4.63	$2^2A'$	3.29	1^2E	2.69		
4^2A	5.61	$3^2A'$	4.25				
5^2A	6.65	$4^2A'$	6.25	3^2A	5.69	2^2A	7.00

[a] Structures are given in Fig.1.

On the other hand, in the high–energy isomers, A1b, A2d and A3h, where all NH$_3$ molecules are bound to Li$^-$ from H sides, the RDs do not change so much from those of Li atom for all states examined. The atomic nature remains in these structures. Thus, their VDEs for the transitions to each neutral state change almost in parallel with one another. The NH$_3$ molecules bound to Li by Li$^-$–H interaction do not affect the electronic character of the cluster very much. The RDs for the 1+1+0 A2b are close to the corresponding values for the 1+0+0 A1a, and the VDEs for each transition in A2b increase a little from those in A1a. We see the analogous relationship in the RDs and the VDEs between the 2+1+0 A3b and the 2+0+0 A2a.

Table 6. Expectation values of radial distribution for unpaired electron (RD, Å) in each neutral state at anionic geometries of Li(H₂O)ₙ ($n \leq 4$).[a] Li is at the origin.

n = 1					n = 2					
W1a		W1b			W2a		W2b		W2c	
1+0+0		0+1+0			2+0+0		1+1+0		1+0+1	
$1^2A'$	2.59	1^2A_1	2.21		$1^2A'$	3.23	1^2A	2.49	$1^2A'$	2.52
$2^2A'$	3.80	2^2A_1	2.66		$2^2A'$	4.09	2^2A	3.18	$2^2A'$	3.35
$1^2A''$	3.30	1^2B_1	2.71		$1^2A''$	4.54	3^2A	3.51	$1^2A''$	3.09
$3^2A'$	3.60	2^2B_2	2.70		$3^2A'$	4.36	4^2A	3.46	$3^2A'$	3.48
$4^2A'$	6.30	3^2A_1	5.78		$4^2A'$	6.41	5^2A	6.18	$4^2A'$	6.17

n = 2					n = 3							
W2d		W2e			W3a		W3b		W3c		W3e	
1+0+1		0+1+1			3+0+0		2+1+0		2+0+1		1+1+1	
1^2A	2.61	$1^2A'$	2.20		1^2A_1	3.81	$1^2A'$	3.08	1^2A	3.61	1^2A	2.47
2^2A	3.43	$2^2A'$	2.62		1^2E	4.81	$2^2A'$	3.87	2^2A	4.11	2^2A	3.31
3^2A	3.54	$1^2A''$	2.66				$1^2A''$	4.28	3^2A	4.42	3^2A	3.06
4^2A	4.26	$3^2A'$	2.66		2^2A_1	5.26	$3^2A'$	3.93	4^2A	5.13	4^2A	3.50
5^2A	6.24	$4^2A'$	5.63		3^2A_1	6.93	$4^2A'$	6.27	5^2A	6.71	5^2A	5.89

n = 3					n = 4					
W3h		W3l			W4a		W4b		W4c	
1+0+2		0+1+2			4+0+0		4+0+0		3+0+1	
$1^2A'$	2.63	1^2A	2.19		1^2A	4.27	1^2A	4.10	$1^2A'$	4.24
$1^2A''$	3.41	2^2A	2.60		2^2A	5.20	2^2A	5.05	$2^2A'$	5.36
$2^2A'$	3.51	3^2A	2.64		1^2E	5.66	3^2A	5.32	$1^2A''$	5.10
$3^2A'$	4.42	4^2A	2.63				4^2A	5.41	$3^2A'$	5.15
$4^2A'$	6.23	5^2A	5.52		3^2A	6.80	5^2A	7.11	$4^2A'$	7.16

[a] Structures are given in Figure 2.

The size dependence of the RDs at the most stable anionic geometries of Li(H₂O)ₙ for each *n* is similar to that of Li(NH₃)ₙ. The one–center (Rydberg–like) ion–pair nature also grows in the structures with the maximum numbers of Li–O bonds. The RD values for the 2²S– and 2²P–like states in W4b (W4a) are roughly double the corresponding values for Li atom. Therefore, we can ascribe the drastic red shifts of the second PES bands for Li⁻(H₂O)ₙ with increasing *n* to this electronic change occurring in the clusters as in the case of Li⁻(NH₃)ₙ.

The increased RD values with *n* in these Li(H₂O)ₙ are similar to that of Na(H₂O)ₙ at the high–energy anionic structures having *n* Na–O bonds. On the other hand, the RDs for W1b, W2e and W3l, where water clusters are bond to Li⁻ from H sides are close to the corresponding atomic values. Thus, the structure dependence of the RDs for Li⁻(H₂O)ₙ resembles well that for Na⁻(H₂O)ₙ. The sharp contrast in the observed size dependence of the PES bands between Li⁻(H₂O)ₙ and Na⁻(H₂O)ₙ actually reflects the different electronic changes occurring at the most stable anionic geometries of these clusters.

3.4 Harmonic Frequencies and IR Intensities for NH and OH Stretches

As we have seen, the electronic nature of Li⁻(NH₃)ₙ and Li⁻(H₂O)ₙ is closely related to their structures. Recent progress in vibrational spectroscopy enables us to determine the cluster

geometries in gas phase. It is thus important to predict theoretically the vibrational feature of the clusters for the further experimental study.

Table 7. Scaled harmonic frequencies[a] (cm^{-1}) and IR intensities (km/mol) for NH stretch bands of Li$^-$(NH$_3$)$_n$ ($n{\leq}4$). Average NH distances (Å) are given in brackets.

Freq.	Int.	Sym.	Freq.	Int.	Sym.	Freq.	Int.	Sym.
NH$_3$		[1.013]	A3a		[1.021]	A4a		[1.021]
3472	5.9	E (v_3)	3359	0.0	A′ (v_3)	3376	1.0	T (v_3)
3329	1.7	A$_1$ (v_1)	3356	27.3	E′ (v_3)	3372	0.0	E (v_3)
			3355	0.0	E″ (v_3)	3371	34.0	T (v_3)
A1a		[1.023]	3352	46.1	A″ (v_3)	3238	0.0	A (v_1)
3333	25.1	E (v_3)	3234	0.0	A′ (v_1)	3237	400.0	T (v_1)
3188	390.5	A$_1$ (v_1)	3220	608.8	E′ (v_1)			
A2a		[1.023]						
3352	8.8	B (v_3)						
3348	18.8	A (v_3)						
3332	8.7	A (v_3)						
3329	51.3	B (v_3)						
3202	94.6	A (v_1)						
3197	842.4	B (v_1)						

[a] Scale factor is 0.943.

Table 8. Scaled harmonic frequencies[a] (cm^{-1}) and IR intensities (km/mol) for OH stretch bands of Li$^-$(H$_2$O)$_n$ ($n{\leq}4$). Average OH distances (Å) are given in brackets.

Freq.	Int.	Sym.	Freq.	Int.	Sym.	Freq.	Int.	Sym.
H$_2$O		[0.960]	W2a		[0.972]	W4b		[0.968]
3815	62.8	B$_2$ (v_3)	3585	319.0	A″ (v_3)	3710	185.2	A (v_3)
3701	13.1	A$_1$ (v_1)	3577	200.8	A′ (v_3)	3653	289.9	A (v_3)
			3470	482.2	A′ (v_1)	3635	154.0	A (v_3)
W1a		[0.972]	3461	1398.8	A″ (v_1)	3604	116.7	A (v_3)
3569	312.5	A″ (v_3)				3599	714.4	A (v_1)
3465	944.6	A′ (v_1)	W3a		[0.971]	3550	675.0	A (v_1)
			3602	0.0	A$_2$ (v_3)	3536	782.8	A (v_1)
			3590	329.3	E (v_3)	3506	701.2	A (v_1)
			3510	34.2	A$_1$ (v_1)			
			3494	1400.9	E (v_1)			

[a] Scale factor is 0.953.

The scaled harmonic frequencies and IR intensities of NH and OH stretches in the free solvents and the cluster anions are summarized in Tables 7 and 8. Symmetric (v_1) and asymmetric (v_3) NH stretch bands of A1a are calculated at 3188 and 3333 cm^{-1}, respectively. They are shifted to the lower frequencies by about 140 cm^{-1} from the corresponding bands of a free NH$_3$. The frequencies of both v_1 and v_3 modes tend to increase gradually as n grows in the larger cluster anions. These frequency changes are correlated with the elongation of the average NH distance from the isolated NH$_3$ to A1a, and with the gradual shortenings of the NH bonds from A1a to A4a. The most intense band is by the symmetric NH stretch in the cluster anions.

Similar frequency shifts are found for Li$^-$(H$_2$O)$_n$. The calculated symmetric and asymmetric OH

http://www.biochempress.com

stretch frequencies of W1a are 3465 and 3569 cm^{-1}, respectively, which are down–shifted by about 240 cm^{-1} from those of a free water molecule. These bands are shifted back gradually to the higher frequencies with the further additions of H_2O molecules. The average OH distance is lengthened by 0.012 Å from H_2O to W1a, and shortened slightly from W1a to W4b. The ν_1–bands are generally more intense than the ν_3–bands in $Li^-(H_2O)_n$.

The frequency lowering of NH and OH stretches in the 1:1 complexes is considered to be due to the slight electron transfer from Li to σ^* orbitals of these bonds as the bond elongation indicates. In fact, if we look back at Figure 3, a large portion of the valence electrons are distributed in the $r \geq$ 2.6 region in bare Li^-, and a small amount of the electrons remains in the NH bond region in A1a. The $N_-(r)$ values for this complex at r_{Li-N} (2.00 Å) and at r_{Li-H} (2.57 Å) are 0.100 and 0.190, respectively (see Table 4). They decrease as n grows and become 0.012 and 0.044 in A4a. The valence electrons from Li^- are squeezed out of $Li^+(NH_3)_n$ core, and less and less electrons remain in the NH bond region with increasing cluster size, which results in the gradual reduction of NH bonds. The size dependence of the OH stretch frequencies can be ascribed to the same reason.

4 CONCLUSIONS

In the present paper, we have analyzed the size dependence of photoelectron spectra for negatively charged $Li^-(NH_3)_n$ and $Li^-(H_2O)_n$ ($n = 1$–4) by *ab initio* molecular orbital method. The conclusions that we have reached are as follows.

(1) The most stable structures of $Li^-(NH_3)_n$ and $Li^-(H_2O)_n$ have as many Li–N or Li–O bonds as possible, which is similar to the solvated Li atoms and cations.

(2) The calculated VDEs for the most stable forms of $Li^-(NH_3)_n$ agree well with the experiment. All observed PES bands of $Li^-(NH_3)_n$ can be assigned to the $2^2S(Li)$–, $2^2P(Li)$– and $3^2S(Li)$–type transitions, respectively, in these structures. The most stable structures of $Li^-(H_2O)_n$ for each n also reproduce well the observed size dependence of the VDEs. The observed first and second PES bands are assignable to the $2^2S(Li)$– and $2^2P(Li)$–type transitions in the structures with n Li–O bonds.

(3) In both $Li^-(NH_3)_n$ and $Li^-(H_2O)_n$ with maximum numbers of Li–nonhydrogen bonds, most valence electrons of Li are squeezed out of the solvation shell. The electronic character of the $n \geq 3$ clusters can be regarded as the state in which the solvated Li^+ is surrounded by the diffuse delocalized electrons. That's why even the fourth solvent molecule can be bound directly to Li against the expectation from the classical octet rule.

(4) At the most stable structures of $Li^-(NH_3)_n$ and $Li^-(H_2O)_n$, the spatial expansion of the unpaired electron with increasing cluster size also proceeds in the neutrals. The growing one–center (Rydberg–like) ion–pair nature is responsible for the rapid decrease in the energy separations

between the neutral ground and excited electronic levels, namely, the red shifts of the higher PES bands.

(5) The structure dependence of the VDEs for $Li^-(NH_3)_n$ and $Li^-(H_2O)_n$ resembles that for Na^- $(NH_3)_n$ and $Na^-(H_2O)_n$. The similar size dependence of the PES bands among $Na^-(NH_3)_n$, $Li^-(NH_3)_n$ and $Li^-(H_2O)_n$, and the different spectral feature of $Na^-(H_2O)_n$ from the other three reflect the similarity and dissimilarity of their most stable structures for each n, in other words, the electronic changes occurring in the clusters with increasing n.

Acknowledgment

5 REFERENCES

[1]   K. Fuke, K. Hashimoto and S. Iwata, Structures, Spectroscopies and Reactions of Atomic Ions With Water Clusters; in: *Advances in Chemical Physics Vol. 110*, Eds. I.Prigogine and S. A. Rice, John Wiley & Sons, New York, 1999, pp. 433–523.

[2]   K. Fuke, K. Hashimoto and R. Takasu, Solvation of Sodium Atom and Aggregates in Ammonia Clusters; in: *Advances in Metal and Semiconductor Clusters*, *Vol.5*, Ed. M. Duncun, Elsevier, Amsterdam, 2001, pp. 1–37.

[3]   I.V. Hertel, C. Huglin, C. Nitsch and C.P. Schulz, Photoionization of $Na(NH_3)_n$ and $Na(H_2O)_n$ Clusters: A Step Towards the Liquid Phase ?, *Phys. Rev. Lett.* **1991**, *67*, 1767–1770.

[4]   F. Misaizu, K. Tsukamoto, M. Sanekata and K. Fuke, Photoionization of clusters of Cs atoms solvated with H_2O, NH_3 and CH_3CN, *Chem. Phys. Lett.* **1992**, *188*, 241–246.

[5]   R. Takasu, K. Hashimoto and K. Fuke, Study on microscopic solvation process of Li atom in ammonia clusters: photoionization and photoelectron spectroscopies of $M(NH_3)_n$ (M=Li, Li^-), *Chem. Phys. Lett.* **1996**, *258*, 94–100.

[6]   R. Takasu, F. Misaizu, K. Hashimoto and K. Fuke, Microscopic Solvation Process of Alkali Atoms in Finite Clusters: Photoelectron and Photoionization Studies of $M(NH_3)_n$ and $M(H_2O)_n$ (M=Li, Li^-, Na^-), *J. Phys. Chem. A* **1997**, *101*, 3078–3087.

[7]   R. N. Barnett and U. Landman, Hydration of Sodium in Water Clusters, *Phys. Rev. Lett.* **1993**, *70*, 1775–1778.

[8]   K. Hashimoto, S. He and K. Morokuma, Structures, stabilities and ionization potentials of $Na(H_2O)_n$ and $Na(NH_3)_n$ ($n=1–6$) clusters. An ab initio MO study, *Chem. Phys. Lett.* **1993**, *206*, 297–304.

[9]   P. Stampfli and K.H.Bennemann, Theory for the solvation of alkali metal atoms in clusters of polar molecules. Many–body polarization interactions, *Comp. Matter. Sci.* **1994**, *2*, 578–584.

[10] G. Markov and A. Nitzan, Solvation and Ionization near a Dielectric Surface, *J. Phys. Chem.* **1994**, *98*, 3459–3466.

[11] K. Hashimoto and K. Morokuma, Ab initio theoretical study of 'surface' and 'interior' structures of the $Na(H_2O)_4$ cluster and its cation, *Chem. Phys. Lett.* **1994**, *223*, 423–430.

[12] K. Hashimoto and K. Morokuma, Ab Initio Molecular Orbital Study of $Na(H_2O)_n$ ($n=1–6$) Clusters and Their Ions. Comparison of Electronic Structure of the 'Surface' and 'Interior' Complexes, *J. Amer. Chem. Soc.* **1994**, *116*, 11436–11443.

[13] K. Hashimoto and K. Morokuma, Ab Initio MO Study of $Na(NH_3)_n$ ($n=1–6$) Clusters and Their Ions: A Systematic Comparison with Hydrated Na Clusters, *J. Amer. Chem. Soc.* **1995**, *117*, 4151–4159.

[14] K. Hashimoto and K. Kamimoto, Theoretical Study of Microscopic Solvation of Lithium in Water Clusters: Neutral and Cationic $Li(H_2O)_n$ ($n=1–6$ and 8), *J. Amer. Chem. Soc.* **1998**, *120*, 3560–3570.

[15] L. M. Ramaniah, M. Bernasconi, and M. Parrinello, Density–functional study of hydration of sodium in water clusters, *J. Chem. Phys.* **1998**, *109*, 6839–6843.

[16] T. Tsurusawa and S. Iwata, Theoretical Studies of Structures and Ionizatoin Threshold Energies of Water Cluster Complexes with a Group 1 Metal, $M(H_2O)_n$ (M = Li and Na), *J. Phys. Chem. A* **1999**, *103*, 6134–6141.

[17] R. Takasu, H. Ito, K. Nishikawa, K. Hashimoto, R. Okuda and K. Fuke, Solvation process of Na_m in small ammonia clusters: photoelectron spectroscopy of $Na_m^-(NH_3)_n$ ($m \leq 3$), *J. Electron. Spectros. Relat. Phenom.* **2000**,

106, 127–139.

[18] R. Takasu, T. Taguchi, K. Hashimoto and K. Fuke, Microscopic solvation process of single Li atom in small water clusters, *Chem. Phys. Lett.* **1998**, *290*, 481–487.

[19] K. Hashimoto, T. Kamimoto and K. Fuke, Ab initio MO study of solvated negative alkali atom clusters: $[M(H_2O)_n]^-$ and $[M(NH_3)_n]^-$ (M = Na and Li, n = 1–3), *Chem. Phys. Lett.* **1997**, *266*, 7–15.

[20] K. Hashimoto, T. Kamimoto and K. Daigoku, Theoretical Syudy of $[Na(H_2O)_n]^-$ (n = 1–4) Clusters: Geometries, Vertical Detachment Energies, and IR Spectra, *J. Phys. Chem. A* **2000**, *104*, 3299–3307.

[21] K. Hashimoto, T. Kamimoto, N. Miura, R. Okuda and K. Daigoku, Theoretical Study of $[Na(NH_3)_n]^-$ (n = 1–4), *J. Chem. Phys.* **2000**, *113*, 9540–9548.

[22] W. J. Hehre, L. Radom, P. v. R. Schleyer, and J. A. Pople, *Ab Initio Molecular Orbital Theory*, Wiley, New York, 1986.

[23] M. J. Frisch, G. W. Trucks, H. B. Schlegel, G. E. Scuseria, M. A. Robb, J. R. Cheeseman, V. G. Zakrzewski, J. A. Montgomery, Jr., R. E. Stratmann, J. C. Burant, S. Dapprich, J. M. Millam, A. D. Daniels, K. N. Kudin, M. C. Strain, O. Farkas, J. Tomasi, V. Barone, M. Cossi, R. Cammi, B. Mennucci, C. Pomelli, C. Adamo, S. Clifford, J. Ochterski, G. A. Petersson, P. Y. Ayala, Q. Cui, K. Morokuma, D. K. Malick, A. D. Rabuck, K. Raghavachari, J. B. Foresman, J. Cioslowski, J. V. Ortiz, A. G. Baboul, B. B. Stefanov, G. Liu, A. Liashenko, P. Piskorz, I. Komaromi, R. Gomperts, R. L. Martin, D. J. Fox, T. Keith, M. A. Al–Laham, C. Y. Peng, A. Nanayakkara, M. Challacombe, P. M. W. Gill, B. Johnson, W. Chen, M. W. Wong, J. L. Andres, C. Gonzalez, M. Head–Gordon, E. S. Replogle, and J. A. Pople, *Gaussian 98, Revision A.9*, Gaussian, Inc., Pittsburgh PA, 1998.

[24] G. Herzberg, *Molecular Spectra and Molecular Structure*, Vol. II, Van Nostrand Reinhold, New York, 1945.

[25] MOLPRO is a package of *ab initio* programs written by H.–J. Werner and P. J. Knowles, with contributions of J. Almlof, R. D. Amos, M. J. O. Deegan, S. T. Elbert, C. Hampel, W. Meyer, K. Peterson, R. Pitzer, A. J. Stone, P. R. Taylor, R. Lindh, M. E. Mura, and T. Thorsteinsson.

[26] H.–J. Werner and P. J. Knowles, A second order multiconfiguration SCF procedure with optimum convergence, *J. Chem. Phys.* **1985**, *82*, 5053–5063.

[27] P. J. Knowles and H.–J. Werner, An efficient second–order MC SCF method for long configuration expansions, *Chem. Phys. Lett.* **1985**, *115*, 259–267.

[28] H.–J. Werner and P. J. Knowles, An efficient internally contracted multiconfiguration–reference configuration interaction method, *J. Chem. Phys.* **1988**, *89*, 5803–5814.

[29] P. J. Knowles and H.–J. Werner, An efficient method for the evaluation of coupling coefficients in configuration interaction calculations, *Chem. Phys. Lett.* **1988**, *145*, 514–522.

[30] K. Mierzwicki and Z. Latajka, Nonadditivity of interaction in $Li(NH_3)_n$ and $Li(NH_3)_n^+$ (n=1–4) clusters, *Chem. Phys.* **2001**, *265*, 301–311.

Biographies

Kenro Hashimoto is an associate professor of information science and computational chemistry at Toyo Metropolitan University (TMU). After obtaining a Ph.D. degree in quantum chemistry from Keio University in September 1989, he moved to the Institute of Physical Chemical Research (RIKEN) as a special researcher, basics science program. He was a research associate with Professor Morokuma at Institute for Molecular Science (IMS) from August 1991 to March 1993. His recent research interests are in the electronic states, reactions and dynamics of clusters, as well as the structures and spectra of weakly bound complexes of atmospheric importance.

Kota Daigoku is a doctor course student in computational chemistry group at TMU. He investigated the solvated electron in ammonium–ammonia complexes during the master course. He has been recently studying the phenol–ammonia clusters in relation to excited state hydrogen transfer.

Tetsuya Kamimoto is a former graduate student in computational chemistry group at TMU. He studied the size dependence of ionization energy of Li–water clusters. After finishing the master course, he moved to IBM Japan.

Taku Shiomsato is a former master course student in computational chemistry group at TMU. He studied the electronic nature of Li–ammonia clusters.